Slip of a one-body dynamical spring-slider model in the presence of slip-weakening friction and viscosity

Jeen-Hwa Wang

Institute of Earth Sciences, Academia Sinica, Taipei, Taiwan

ABSTRACT

This study is focused on analytic study at small displacements and numerical simulations of slip of a one-body dynamical slider-slider model in the presence of slip-weakening friction and viscosity. Analytic results with numerical computations show that the displacement of the slider is controlled by the decreasing rate, γ, of friction force with slip and viscosity, η, of fault-zone material. The natural period of the system with slip-weakening friction and viscosity is longer than that of the system without the two factors. There is a solution regime for η and γ to make the slider slip steadily without strong attenuation. The viscous effect is stronger than the frictional effect. Meanwhile, a change of η results in a larger effect on the slip of the slider than a change of γ. Numerical simulations are made for a one-body dynamical slider-slider model in the presence of three slip-weakening friction laws, i.e., the thermal-pressurization (TP) friction law, the softening-hardening (SH) friction law, and a simple slip-weakening (SW) friction law, and viscosity. Results show that slip-weakening friction and viscosity remarkably affect slip of the slider. The TP and SW friction laws cause very similar results. The results caused by the SH friction law are quite different from those by the other two. For the cases in study, the fixed points are not an attractor.

1. Introduction

Essentially, the rupture processes of an earthquake consist of three steps: nucleation (or initiation), dynamical propagation, and arrest. It is necessary to study the mechanisms controlling the whole rupture processes. Such processes are very complicated, and cannot be completely solved just using a simple model. Several factors, including brittle-ductile fracture rheology [Jeffreys 1942; Scholz 1990], normal stress [Fang et al. 2011], re-distribution of stresses after fracture, the geometry of faults [Fang et al. 2011], friction [Nur 1978; Dieterich 1979; Ruina 1983], distribution of frictional strengths [Wang and Hwang 2001; Wang 2008], healing from dynamic to static friction after an earthquake [Wang 1997], pore fluid pressure [Scholz 1990; Wang 2009, 2011]; elastohydromechanic lubrication [Brodsky

and Kanamori 2001; Garagash and Germanovich 2012]; thermal pressurization [Rice 2006; Bizzarri 2011a, 2011b], stress corrosion [Anderson and Grew 1977; Atkinson 1984], and metamorphic dehydration [Brantut et al. 2011], will control earthquake ruptures.

Friction is one of the most important factors in controlling the rupture processes of an earthquake [Nur 1978; Dieterich 1979; Ruina 1983; Cao and Aki 1986; Knopoff et al. 1992; Rice 1993; Wang 1996, 1997, 2007, 2012; Rubin and Ampuero 2005; Ampuero and Rubin 2008; Bizzarri 2011c; Bhattacharya and Rubin 2014]. The friction coefficient, f, is defined as the ratio of shear stress, τ, to the effective normal stress, σ_{eff}, on the fault plane. Laboratory rock sliding experiments [Byerlee 1978] show that for most rock types, the friction coefficient at which slip initiates is about 0.6-0.8. At lithostatic normal stress and hydrostatic pore pressure, observations suggest that the shear strength of faults exceeds ~100 MPa at seismogenic depths on continental strike-slip faults. The frictional force between two contact planes is classically considered to drop from static one to dynamic one after the two planes move relatively. Indeed, the friction law that has been mainly inferred from laboratory experiments is quite complicated and not completely understood, especially for that on natural faults due to a lack of observational constraints. This makes the proper constitutive law for fault friction an elusive mathematical formulation. Dieterich [1972] first found time-dependent static frictional strength of rocks in laboratory experiments. Dieterich [1979] and Shimamoto [1986] observed velocity-dependent frictional strengths. Dieterich [1979] and Ruina [1983] proposed empirical, velocity- and state-dependent friction laws. There are two state evolution laws, i.e., "aging" and "slip" versions. Essentially, velocity- and state-dependent friction includes two different processes: the velocity-weakening process and the velocity-hardening

one. In fact, a large debate related to the friction laws governing earthquake ruptures has been made for a long time. Although this problem is important, it is out of the scope of this article and thus will not be explained in details. A detailed description of the generalized velocity- and state-dependent friction law and the debates can be found in several articles [Marone 1998; Wang 2002; Bizzarri and Cocco 2006c; Bizzari 2011c].

Several simple friction laws have been taken into account by some researchers. Burridge and Knopoff [1967] first considered a velocity-dependent, weakening-hardening friction law. Carlson and Langer [1989] proposed a purely nonlinearly velocity-weakening friction law which was also used by others [Carlson 1991; Carlson et al. 1991; Beeler et al. 2008] to theoretically model earthquakes. Wang [1995, 1996, 2012] considered a piecewise, linearly velocity-dependent weakening- hardening friction, which is simplified from the friction law proposed by Burridge and Knopoff [1967]. The decreasing (weakening) and increasing (hardening) rates of dynamic friction with sliding velocity are two main parameters of this friction law. Cao and Aki [1984/85] took a displacement softening-hardening friction law.

Cochard and Madariaga [1994] and Madariaga and Cochard [1994] assumed that purely velocity-dependent friction models can lead to unphysical phenomena or mathematically ill-posed problems. This means that the velocity-dependent friction law is very unstable at low velocities both during the passage of the rupture front and during the possible slip arrest phase. Moreover, Ohnaka [2003] stressed that purely velocity-dependent friction is in contrast with laboratory evidence, that is, the friction law is not a one-valued function of velocity. Bizzarri [2011c] deeply discussed this point.

Brune [1979] showed that frictional sliding at $\tau \approx 10$ MPa would produce a heat flow anomaly that is not observed in field data adjacent to the San Andreas fault [Lachenbruch 1980]. Temperature measurements in boreholes drilled across faults shortly after earthquakes also indicate low shear traction during seismic slip [Kano et al. 2006; Wang 2006, 2011). Since Lachenbruch [1980] pointed out the heat-flux paradox, numerous studies have been placed on the thermal properties of the fault-zone rocks to address the importance of thermal effect during earthquake ruptures [Chester and Higgs 1992; Fialko 2004; Bizzarri and Cocco 2006a, 2006b; Wang 2006, 2007, 2009, 2011; Bizzarri 2011a, 2011b; Bizzarri and Crupi 2013]. Sibson [2003] also stressed the presence of pseudotachylytes [Sibson 1975] due to heating during earthquake ruptures. Numerous studies have conducted on modeling the frictional heat produced during seismic sliding. Theoretical studies on the spontaneous propagation of earthquake ruptures

on 3D faults by Bizzarri and Cocco [2006a, 2006b] revealed that melting of rocks and fault gouge is likely to occur even with the inclusion of the thermal pressurization of pore fluids. Moreover, the dramatic fault weakening at high slip rates predicted by the flash heating of micro-asperity contacts is not able to avert melting [Bizzarri 2009].

When fluids are present in faults, thermal pressurization can play a significant role on earthquake rupture and also result in resistance on the fault plane [Sibson 1973; Fialko 2004; Bizzari and Cocco 2006a, 2006b; Rice 2006; Wang 2009, 2011, 2013; Bizzarri 2010; Bizzarri 2011a, 2011b]. Rice [2006] proposed two end-members models for thermal pressurization: the adiabatic-undrained-deformation (AUD) model and slip-on-a-plane (SOP) model. He also obtained the shear stress-slip functions caused by the two models.

In spite of a large number of fault-governing friction laws, the only constitutive law able to avoid the melting is a slip- and velocity-weakening friction law [Sone and Shimamoto 2009; Bizzarri 2010], for which the fault weakening is so dramatic that it cannot be counterbalanced by the resulting enhanced slip velocities. However, both thermal pressurization of pore fluids and flash heating predict not only a very dramatic stress drop, but also a very high peak in fault slip velocity, so that the final result is that melting temperature is very often exceeded, unless the slipping zone (where the deformation is concentrated) is extremely large [Bizzarri and Cocco 2006b; Bizzarri 2009]. Bizzarri [2011a] stressed that when melting occurs, the rheological behavior of the fault zone no longer obeys the Coulomb–Amonton–Mohr formulation, in that a viscous rheology is needed to describe the traction evolution during the ruptures.

Jeffreys [1942] first emphasized the influence of viscosity on faulting. Viscosity can also be controlled by the presence of frictional melts in fault systems [Byerlee 1968]. Temperature, pressure, water content, etc., will influence viscosity [Turcotte and Schubert 1982]. Scholz [1990] suggested that the residual strength of fault-generated friction melts would be high and so present significant viscous resistance to shear. This inhibits continued slip. On the other hand, Spray [1993, 1995] stated that most pseudotachylytes are partial melts possessing low viscosity, and capable of generating a sufficient melt volume to reduce the effective normal stress. Thus, friction melts can act as fault lubricants during co-seismic slip [Spray 2005]. His results show that viscosity remarkably decreases with increasing temperature. Rice et al. [2001] discussed the physical basis of velocity- and state-dependent friction, including the direct effect in thermally activated processes al-

lowing creep slippage at asperity contacts on the fault surface. Wang [2007] stressed the viscous effect on earthquake ruptures from the comparison between simulated waveforms and seismograms recorded near the Chelungpu fault of the 1999 Chi-Chi, Taiwan, earthquake. Wang [2011] assumed that quartz plasticity could be formed in the main slip zone of the 1999 Chi-Chi, Taiwan, earthquake when $T > 300°C$ after the fault ruptured. The shear zone with quartz plasticity would be localized in a 5-mm thick heated layer. Quartz plasticity could lubricate the fault plane at higher T and yield viscous stresses to resist slip at lower T. On the other hand, several researchers [Knopoff et al. 1973; Cohen 1979; Xu and Knopoff 1994; Knopoff and Ni 2001; Dragoni and Santini 2015] took the viscous effect as a factor in causing seismic radiation to reduce energy during earthquake ruptures.

Dragoni and Santini [2015] considered with two-degrees-of-freedom dynamical spring-slider model to approach two asperities on a fault. Except for the coupling between two sliders, the equation of motion of a slider in their model is essentially the same as that used in this study. Hence, their studies are explained in details more or less here. They introduced a term proportional to slip rate in the equations of motion to represent seismic radiation during the slipping modes. They gave a complete analytical solution of the four dynamic modes of the system. Any seismic event can be expressed as a sequence of modes, for which the moment rate, the spectrum and the total seismic moment can be calculated. They also considered the energy budget of the event and calculated its seismic efficiency. Seismic radiation might change the evolution of the system from a given state, since it moves the boundaries between the different subsets of the sticking region. In addition, the slip amplitude in a seismic event is smaller, while the slip duration is longer in the presence of radiation (or viscosity). The shape of the moment rate function depends on the seismic efficiency and the seismic moment decreases with increasing efficiency at constant radiated energy (or constant viscosity).

Since the ingredients of an ideal model are only partly understood, a set of equations to describe comprehensively fault dynamics has not yet been established. Nevertheless, some models, for instance the crack model and dynamical lattice model, have been developed to approach fault dynamics for a long time. Although the frictional effect on earthquake ruptures has been widely studied as mentioned above, the studies of viscous effect on earthquake ruptures are few. The viscous effect mentioned in Rice et al. [2001] was just an implicit factor included in the direct effect of friction law. In this work, I will explore the effects of slip-weakening friction, especially due to thermal pressurization, and viscosity on earthquake ruptures on the basis of a one-body spring-slider model, which is used to approach an earthquake fault. The viscous effect is represented by an explicit parameter. Results will be applied to understand earthquake ruptures.
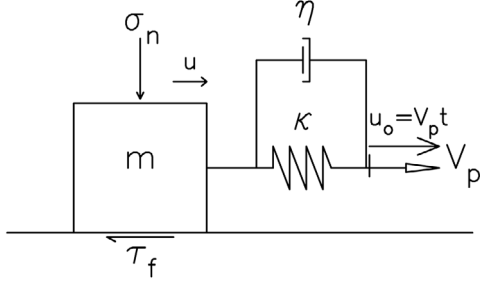
2. Model

One-body spring-slider model
The equation of motion of the one-body dynamical spring-slider model (see Figure 1) is:

$$md^2u/dt^2 = -K(u - v_p t) - F(u,v) - \Phi(v), \tag{1}$$

where m is the mass of the slider, u is the displacement of the slider, K is the spring constant, v_p is the speed of the driving force, $v = du/dt$ is the velocity of the slider, F is the frictional force between the slider and the background and could be a function of u and v, and Φ is the viscous force between the slider and the background and is a function of v. The slider is pulled by a leaf spring of strength, K, with a constant velocity, v_p, which represents the speed of a moving plate. When the driving force, $Kv_p t$ is slightly larger than the static frictional force, F_o, friction changes from static friction strength to dynamic one.

Viscosity
For deformed materials, there are two components, i.e., elastic component and viscous component, when the viscous effect is present. The elastic component can be modeled as a spring with an elastic constant E, given by the formula: $\sigma = E\varepsilon$, where σ, E, and ε are, respectively, the stress, the elastic modulus of the material, and the strain that occurs under the given stress. The viscous component can be modeled as a dashpot such that the stress–strain rate relationship can be given as, $\sigma = v(d\varepsilon/dt)$ where v is the viscosity of the material. There are two models to describe the viscous materials (cf. Hudson [1980]). The first one is the Maxwell model which can be represented by a purely viscous damper (denoted by "D") and a purely elastic spring (denoted by "S") connected in series, as shown in Figure 1. The model can be represented by the following equation: $d\varepsilon/dt = d\varepsilon_D/dt + d\varepsilon_S/dt = \sigma/v + E^{-1}d\sigma/dt$. If the material is put under a constant strain, the stresses gradually relax. When a material is put under a constant stress, the strain has two components. First, an elastic component occurs instantaneously, corresponding to the spring, and relaxes immediately upon release of the stress. The second is a viscous component that grows with time as long as the stress is applied. The Maxwell

Figure 1. One-body spring-slider model. In the figure, u, K, η, v_p, N, and F denote, respectively, the displacement, the spring constant, the coefficient of viscosity, the velocity of the driving force, the normal force, and the frictional force.

model predicts that stress decays exponentially with time. One limitation of this model is that it does not predict creep accurately.

The second one is the Kelvin-Voigt model, also known as the Voigt model, consists of a Newtonian damper and Hookean elastic spring connected in parallel, as shown in Figure 1. It is used to explain the creep behavior of materials. The constitutive relation is expressed as: $\sigma(t) = E\varepsilon(t) + v d\varepsilon(t)/dt$, which represents a solid undergoing reversible, viscoelastic strain. Upon application of a constant stress, the material deforms at a decreasing rate, asymptotically approaching the steady-state strain. When the stress is released, the material gradually relaxes to its un-deformed state. At constant stress (creep), the model is quite realistic as it predicts strain to tend to σ/E as time continues to infinity. The model is extremely good with modeling creep in materials, but with regards to relaxation the model is much less accurate.

Although viscosity varies with temperature, pressure, and water content, only a constant viscosity for each segment is considered below. The Newtonian viscous force is described by a dash-pot shown in Figure 2 specified with viscosity v between the slider and the moving plate, and, thus, the viscous force at the slider is represented by $-vv$ where v is the velocity of the slider. For the Kelvin-Voigt model, the stress is a function of both strain and strain rate and thus can be applied to the seismological problems [Hudson 1980].

However, it is not easy to directly implement viscosity in a dynamical system as used in this study. Hence, viscosity is here represented in an alternative way. Viscosity leads to the damping of oscillations of a body. The damping coefficient is usually proportional to viscosity and is controlled by the linear dimension of the body in a viscous fluid. For example, according to Stokes' law, the damping coefficient η of a sphere of radius R in a fluid of viscosity v is given by $\eta = 6\pi Rv$ (cf. Kittel et al. [1968]). In order to simplify the problem, the damping coefficient is regarded as viscosity hereafter. Hence, the viscous force is $\Phi = \eta v$. Noted that the unit of η is N/(m/s).

Friction due to thermal pressurization

Equation (1) exhibits that the motion of the slider is controlled by the frictional force, $F(u,v)$. As mentioned above, friction can also be produced from thermal pressurization. On a fault plane with an area of A and an average displacement $\bar{u}$, the frictional energy caused by the dynamic friction stress, τ_d, is $E_f = \tau_d \bar{u} A$ which could result in a temperature rise, ΔT. Frictional heat can conduct outwards from the slipping zone to wall rocks. Theoretical analyses [Fialko 2004; Bizzari and Cocco 2006a, 2006b] show that T is described by an error function of distance and decays outwards from the fault plane. Under thermal pressurization, the energy and fluid mass conservation equations in a 1-D fault plane, in which the x- and y-axes denote the directions along and normal to the fault plane, respectively, can be found in Rice [2006].

Rice [2006] proposed two end-members models for thermal pressurization: the adiabatic-undrained-deformation (AUD) model and slip-on-a-plane (SOP) model. The first model corresponds to a homogeneous simple shear strain at a constant normal stress σ_n on a spatial scale of the sheared layer that is broad enough to effectively preclude heat or fluid transfer. The second model shows that all sliding is on the plane with $\tau(0) = f(\sigma_n - p_o)$ where p_o is the pore fluid pressure on the sliding plane $(y = 0)$. For this second model, heat is transferred outwards from the fault plane. The shear stress- slip functions, $\tau(u)$, caused by thermal pressurization [Rice 2006] are: (a) $\tau_{aud}(u) = f(\sigma_n - p_o)\exp(-u/u_c)$ for the AUD model; and (b) $\tau_{sop}(u) = f(\sigma_n - p_o)\exp(u/L^*)erfc(u/L^*)^{1/2}$ for the SOP model, The two parameters u_c and L^* are the respective characteristic displacements, which are in terms of physical properties of the fault-zone materials, to control the shear stress-slip functions of the individual end-member models. For the AUD model, u_c is associated with the thickness of fault zone and a characteristic displacement of the shear stress-slip function. For the SOP model, Rice [2006] addressed that there is not a char-

a: Kevin−Voigt Model   b: Maxwell Model
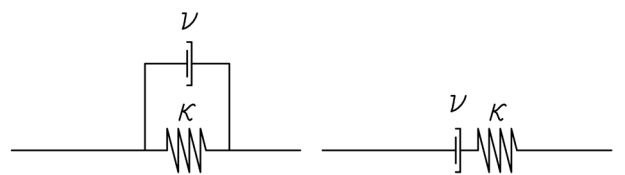
Figure 2. The two types of viscous materials: (a) for the Kelvin–Voigt model and (b) for the Maxwell model. (κ = spring constant and v = coefficient of viscosity).

acteristic displacement for the shear stress-slip function. The stress $\tau_{aud}(u)$ displays exponentially slip-weakening friction. Indeed, The stress $\tau_{sop}(u)$ also shows slip-weakening [Wang 2009]. Since the SOP model is based on a constant velocity, it is not appropriate in this study.

In order to perform the analytical study of the frictional effect on earthquake ruptures based on the one-body spring-slider model, a simplified linearly slip-weakening friction law in the form of $F(u) = F_o - \gamma u$ [Wang 2016], where γ is the weakening rate, is considered hereafter. This leads to the marginal analyses of slip of one-body spring-slider model in the presence of friction, and the results could work for slow earthquakes. For numerical simulations of the dynamical model, a slip-weakening friction law (denoted by the TP friction law hereafter): $F(u) = F_o \exp(-u/u_c)$, where u_c is a characteristic displacement, from the stress-slip function of the AUD model, is first taken into account. In addition, the displacement softening-hardening friction law (denoted by the SH friction law hereafter): $F(u) = F_o \exp[-(u^2 - u_c^2)/c^2]$, where F_o, u_o, and c are constants, used by Cao and Aki [1984/85] is considered. For the purpose of comparison, a slip-weakening friction law (denoted by the SW friction law hereafter): $F(u) = F_o/(1+u/u_c)$ similar to the velocity-weakening friction law: $F(u) = F_o/(1+v/v_c)$, where F_o is the static frictional force and v_c is the characteristic velocity, proposed by Carlson and Langer [1989] is also used. The functions of normalized friction force versus displacement for the three slip-weakening friction laws, with $u_c = 0.1$ m and $c = 0.3$ m, are displayed in Figure 3. Obviously, the SH friction law that increases slightly with slip and then decreases with increasing slip is quite different from the other two. For the given values of u_c and c, the value of SH friction is higher than those of SW and TP friction when the displacement is shorter than a certain value. The value of SW friction is higher than that that of TP friction and the difference between them increases with displacement. Obviously, the TP friction law leads to a faster drop of friction and a higher stress drop than the other two.

3. Analytical studies

Substituting the simplified slip-weakening friction law, i.e., $F(u) = F_o - \gamma u$, and viscous force, i.e., $\Phi(v) = \eta v$, into Equation (1) leads to

$$m d^2 u / dt^2 = -K(u - v_p t) - F_o + \gamma u - \eta v. \qquad (2)$$

When the driving force, $K v_p t$ is slightly larger than F_o, the frictional force changes from static one to dynamic one and thus the slider moves. Since the duration time of an earthquake rupture is usually short and
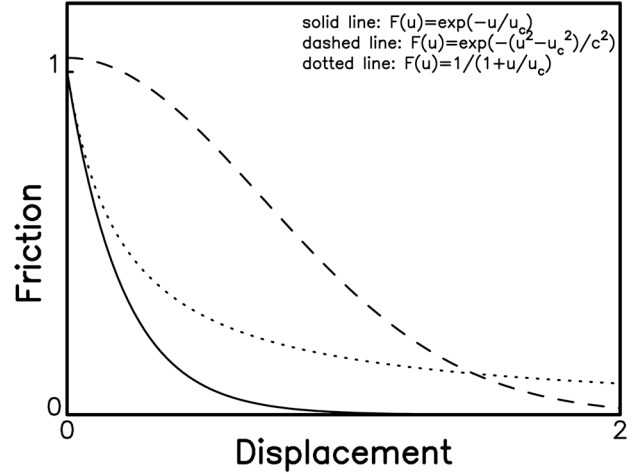
Figure 3. Three slip-weakening friction laws: the solid line for $F(u) = 1/(1+u/u_c)$ with $u_c = 0.1$ m; the dashed line for $F(u) = \exp[-(u^2 - u_c^2)/c^2]$ with $u_c = 0.1$ m and $c = 0.3$ m; and the dotted line for $F(u) = 1/(1+u/u_c)$ with $u_c = 0.1$ m.

$v_p (\approx 10^{-11}$ m/s$)$ is also very small, the value of $K v_p t$ during an earthquake can be ignored. Hence, the equation of motion becomes:

$$m d^2 u / dt^2 + \eta du / dt + (K - \gamma)u = 0. \qquad (3)$$

Inserting the trail solution $e^{i\alpha t}$ into Equation (3) leads to

$$m\alpha^2 - i\eta\alpha - (K - \gamma) = 0. \qquad (4)$$

The solutions of Equation (4) are

$$\alpha = (i\eta/2m) \pm [K/m - (\eta^2 + 4m\gamma)/4m^2]^{1/2}. \qquad (5)$$

Inserting Equation (5) into $e^{i\alpha t}$ leads to $e^{-\eta t/2m}\exp\{\pm i[(K/m) - (\eta^2 + 4m\gamma)/4m^2]^{1/2}t\}$. The first term shows attenuation of slip with time and the second one represents the slip of the slider. The slip remarkably decreases when viscosity is high or the mass of the slider is small. Let $\omega_o = (K/m)^{1/2}$ be the natural angular frequency of the one-body spring-slider system without friction and viscosity. The natural period is $T_o = 2\pi/\omega_o = 2\pi(m/K)^{1/2}$. The natural angular frequency of the present system with friction and viscosity is

$$\omega_n = [\omega_o^2 - (\eta^2 + 4m\gamma)/4m^2]^{1/2}. \qquad (6)$$

Equation (6) indicates that ω_n is an imaginary number when $\omega_o < (\eta^2 + 4m\gamma)^{1/2}/2m$. Together with the term $e^{-\eta t/2m}$, this inequality results in thorough attenuation of slip. Hence, the condition of $\omega_o > (\eta^2 + 4m\gamma)^{1/2}/2m$ is necessary for the existence of stable slippage of the slider. Under this condition, ω_n is lower than ω_o. In other words, the natural period of the system, i.e., $T_n =$

$2\pi/\omega_n$, is

$$T_n = T_o/[1 - T_o^2(\eta^2 + 4m\gamma)/(4\pi m)^2]^{1/2}. \tag{7}$$

Obviously, T_n is longer than T_o and increases with η and γ, thus indicating that friction and viscosity both lengthen the natural period of the system.

In order to further describe the condition: $\omega_o > (\eta^2 + 4m\gamma)^{1/2}/2m$, this inequality is re-written as $mK > (\eta/2)^2 + m\gamma$. Figure 4 displays the curve of parabolic equation: $\eta^2 + 4m\gamma = 4mK$. This gives $\gamma = K$ when $\eta = 0$ and $\eta^2 = 2(mK)^{1/2}$ when $\gamma = 0$. Since the four parameters are all positive, the values of η and γ that lead to a real value of ω_n for stable slippage of the slider must be inside the range (called the solution regime) below the curve.

Let the general solution of Equation (3) be $u(t) = C_1\exp(i\alpha_1 t) + C_2\exp(i\alpha_2 t)$ with $\alpha_1 = i\eta/2m + \omega_n$ and $\alpha_2 = i\eta/2m - \omega_n$. This gives $u(t) = e^{-\eta t/2m}[C_1\exp(i\omega_n t) + C_2\exp(-i\omega_n t)]$. The velocity of the slider is $v(t) = (-\eta/2m)e^{-\eta t/2m}[C_1\exp(i\omega_n t) + C_2\exp(-i\omega_n t)] + i\omega_n e^{-\eta t/2m} \times [C_1\exp(i\omega_n t) + C_2\exp(-i\omega_n t)]$. In order to solve the problem, the initial conditions are: (1) the displacement of the slider is null at $t = 0$, i.e., $u(0) = 0$; and (2) the initial velocity is v_o at $t = 0$, i.e., $v(0) = v_o$. The lower bound of v_o should be v_p because the plate motion is always in operation. This gives

$$C_1 + C_2 = 0; \tag{8a}$$

$$(-\eta/2m + i\omega_n)C_1 - (\eta/2m + i\omega_n)C_2 = v_o. \tag{8b}$$

The solutions of Equation (8) are $C_1 = v_o/2i\omega_n$ and $C_2 = -v_o/2i\omega_n$. Inserting the solutions with C_1 and C_2 into Equation (3) leads to $u(t) = e^{-\eta t/2m}(v_o/\omega_n)[\exp(i\omega_n t) - \exp(-i\omega_n t)]/2i$. This gives
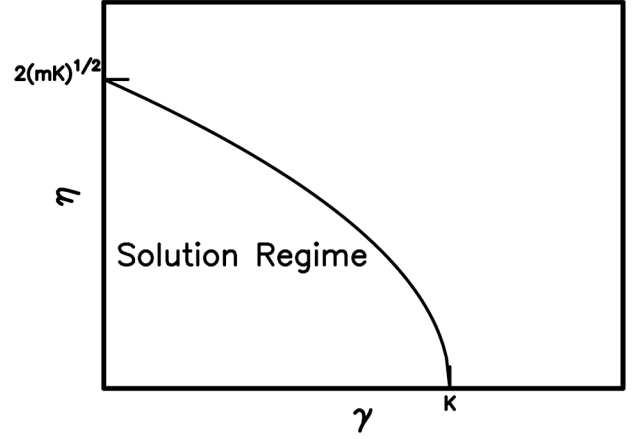

Figure 4. The solution regime of η and γ based on K described by the parabolic equation: $\eta^2 + 4m\gamma = 4mK$ for the one-body spring-slider model.

$$u(t) = (v_o/\omega_n)e^{-\eta t/2m}\sin(\omega_n t), \tag{9}$$

where the ratio v_o/ω_n denotes the amplitude of slip function and varies with four model parameters. The value of $u(t)$ increases with time, reaches the peak value and then decreases with time. The peak value of $u(t)$ with $v(t) = 0$ occurs at time $t_p = tan^{-1}(2m\omega_n/\eta)$.

In order to schematically demonstrate Equation (9) in terms of γ and η, a few computational examples for the normalized displacement, i.e., $u(t)/(v_o/\omega_n)$, with $K = 10$ nt/m and $m = 10$ kg, which lead to $\omega_o = 1$ Hz or $T_o = 2\pi$ sec, are given below. Based on Figure 3, γ and η must be smaller than 10 nt/m and 20 nt/(m/s), respectively, when $K = 10$ nt/m and $m = 10$ kg. Figure 5 exhibits $u(t)/(v_o/\omega_n)$ for five values of γ, i.e., 0, 2, 4, 6, and 8 nt/m, when $\eta = 0$ nt/(m/s). Since the displacement decays very fast with η, only $u(t)/(v_o/\omega_n)$ for five small values of η, i.e., 0.0, 0.2, 0.4, 0.6, and 0.8 nt/(m/s), when $\gamma = 1$ nt/m are displayed in Figure 6. In Figures 5 and 6,
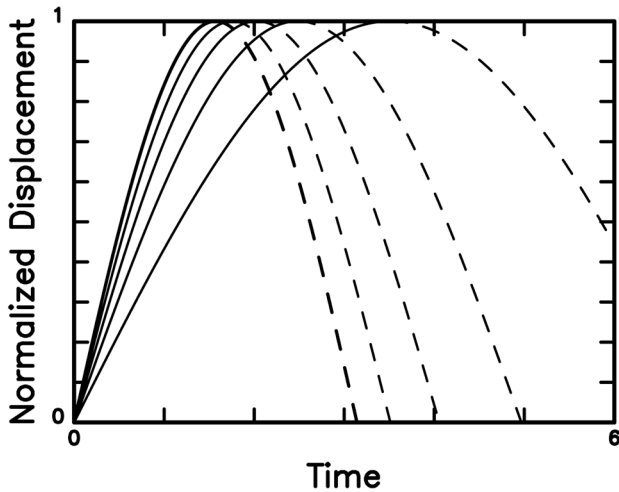

Figure 5. The slip of the slider for five values of γ, i.e., 0, 2, 4, 6, 8 N/m (from left to right), when $K = 10$ N/m, $m = 10$ kg, and $\eta = 0$.
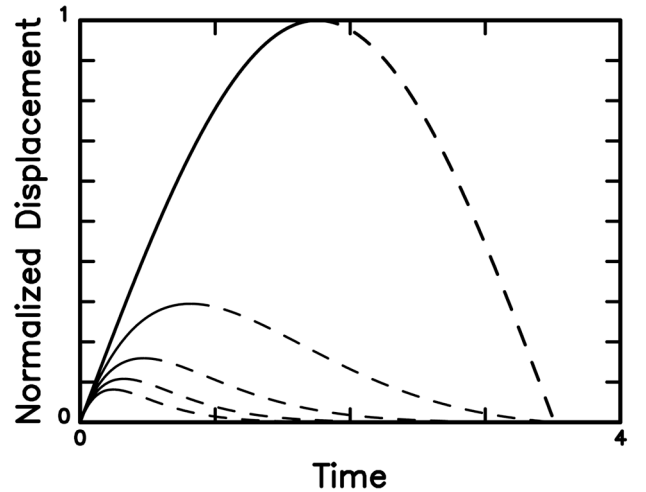

Figure 6. The slip of the slider for five values of η, i.e., 0.0, 0.2, 0.4, 0.6, 0.8 N/(m/s) (upside down), when $K = 10$ N/m, $m = 10$ kg, and $\gamma = 1$ N/m.

the normalized displacements for $t > t_p$ are displayed by dashed lines, because the slider stops when $v(t_p) = 0$. It is noted that since ω_n decreases with η and γ, the actual amplitude should increase with both η and γ.

4. Numerical simulations

In numerical simulations, above-mentioned non-linear friction laws with linear viscous law are taken into account. Substituting the TP friction law and the viscous law into Equation (3) leads to

$$md^2u/dt^2 = -K(u - v_p t) - F_o \exp(-u/u_c) - \eta v. \quad (10)$$

In order to easily perform numerical computations, Equation (10) must be normalized. The normalization parameters are: $D_o = F_o/K$, $U = u/D_o$, $U_c = u_c/D_o\omega_o$, and $V_p = v_p/D_o\omega_o$ and $\tau = (K/m)^{1/2}t = \omega_o t$. This gives $d\tau = \omega_o dt$, $du/dt = [F_o/(mK)^{1/2}]dU/d\tau$, $d^2u/dt^2 = (F_o/mK) d^2U/d\tau^2$, $A = d^2U/d\tau^2$, and $V = dU/d\tau$. In addition, $\eta/(mK)^{1/2}$ is simply denoted by η below. Clearly, all normalized parameters are dimensionless. Hence, Equation (10) becomes:

$$d^2U/d\tau^2 = -U - \eta dU/d\tau - \exp(-U/U_c) + V_p\tau. \quad (11)$$

Let $y_1 = U$ and $y_2 = dU/d\tau$. Equation (11) can be re-written as two first-order differential equations:

$$dy_1/d\tau = y_2 \quad (12a)$$

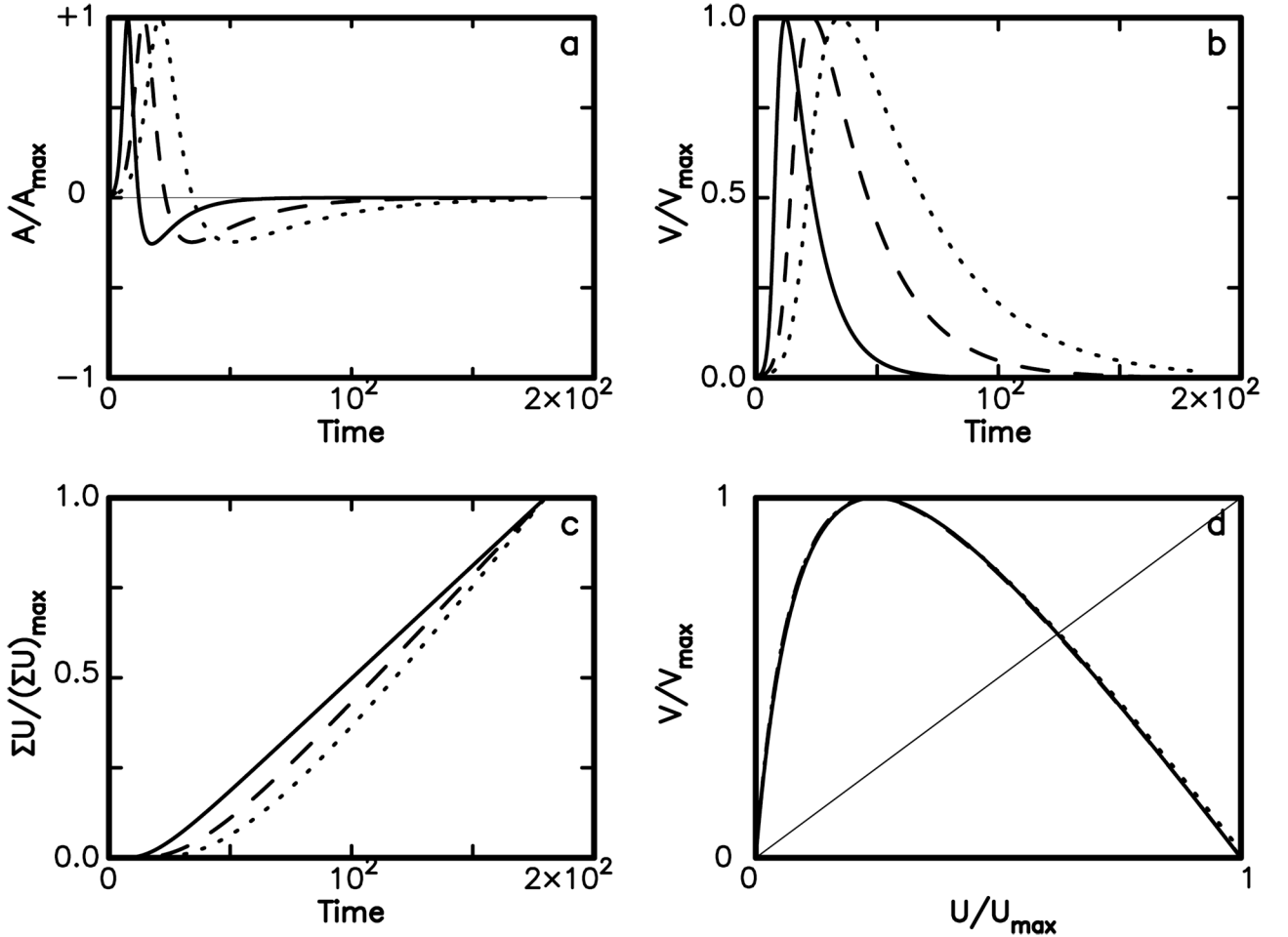$$dy_2/d\tau = -y_1 - \eta y_2 - \exp(-y_1/U_c) + V_p\tau. \quad (12b)$$

For the SH friction law, Equation (11) can be normalized and re-written as two first-order differential equations with the normalized parameters:

$$dy_1/d\tau = y_2 \quad (13a)$$

$$dy_2/d\tau = -y_1 - \eta y_2 - \exp[-(y_1^2 - U_c^2)/\chi^2] + V_p\tau. \quad (13b)$$

where $\chi = c/D_o$.

For the SW friction law, Equation (11) can be normalized and re-written as two first-order differential equations with the normalized parameters:

Figure 7. The time sequences of normalized acceleration (A/A_{max}), normalized velocity (V/V_{max}), and normalized cumulative displacement $\Sigma U/(\Sigma U)_{max}$ and the phase portrait of V/V_{max} versus U/U_{max} of the slider, acted by TP friction of $F(U) = \exp(-U/U_c)$, for $\eta = 10$ (solid line), 20 (dashed line), and 30 (dotted line) when $U_c = 1$.

$$dy_1/d\tau = y_2 \tag{14a}$$

$$dy_2/d\tau = -y_1 - \eta y_2 - 1/(y_1 + U_c) + V_p\tau. \tag{14b}$$

Equations (12)-(14) will be numerically solved using the fourth-order Runge-Kutta method (cf. Press et al. [1986]). It is noted that only the positive displacement is considered in this study, because the negative values of slip are usually not admitted in seismological applications. For each friction law, four diagrams are produced from numerical simulations: the time variations in normalized acceleration, A/A_{max}, the time variations in normalized velocity, V/V_{max}, the time variations in normalized cumulative displacement, $\Sigma U/(\Sigma U)_{max}$, where ΣU denotes the cumulative displacement, and the phase portrait of V/V_{max} versus U/U_{max}.

A phase portrait, denoted by $y = f(x)$, is a plot of a physical quantity versus another of an object in a dynamical system [Thompson and Stewart 1986]. The intersection point of the bisection line, i.e., $y = x$, and $f(x)$ is called the fixed point, that is, $f(x) = x$. If the function $f(x)$ is continuously differentiable in an open domain

near a fixed point x_f and $|f'(x_f)| < 1$, attraction is generated. In other words, an attractive fixed point is a fixed point x_f of a function $f(x)$ such that for any value of x in the domain that is close enough to x_f, the iterated function sequences, i.e., $x, f(x), f^2(x), f^3(x),\ldots$, converges to x_f. An attractive fixed point is a special case of a wider mathematical concept of attractors. Chaos can be generated at some attractors. The details can be seen in Thompson and Stewart [1986] or other nonlinear literatures.

Figure 7 displays the time variations in A/A_{max}, V/V_{max}, and $\Sigma U/(\Sigma U)_{max}$ and the phase portrait of V/V_{max} versus U/U_{max} with $\eta = 10$ (solid line), 20 (dashed line), and 30 (dotted line) when $U_c = 0.1$ for the TP friction law. This figure shows the viscous effect. Figure 8 displays the time variations in A/A_{max}, V/V_{max}, and $\Sigma U/(\Sigma U)_{max}$ and the phase portrait of V/V_{max} versus U/U_{max} for the TP friction law with $U_c = 0.1$ (solid line), 0.3 (dashed line), and 0.5 (dotted line) when $\eta = 10$. Figure 9 displays the time variations in A/A_{max}, V/V_{max}, and $\Sigma U/(\Sigma U)_{max}$ and the phase portrait of V/V_{max} versus U/U_{max} for the SW friction law with $U_c = 0.1$ (solid
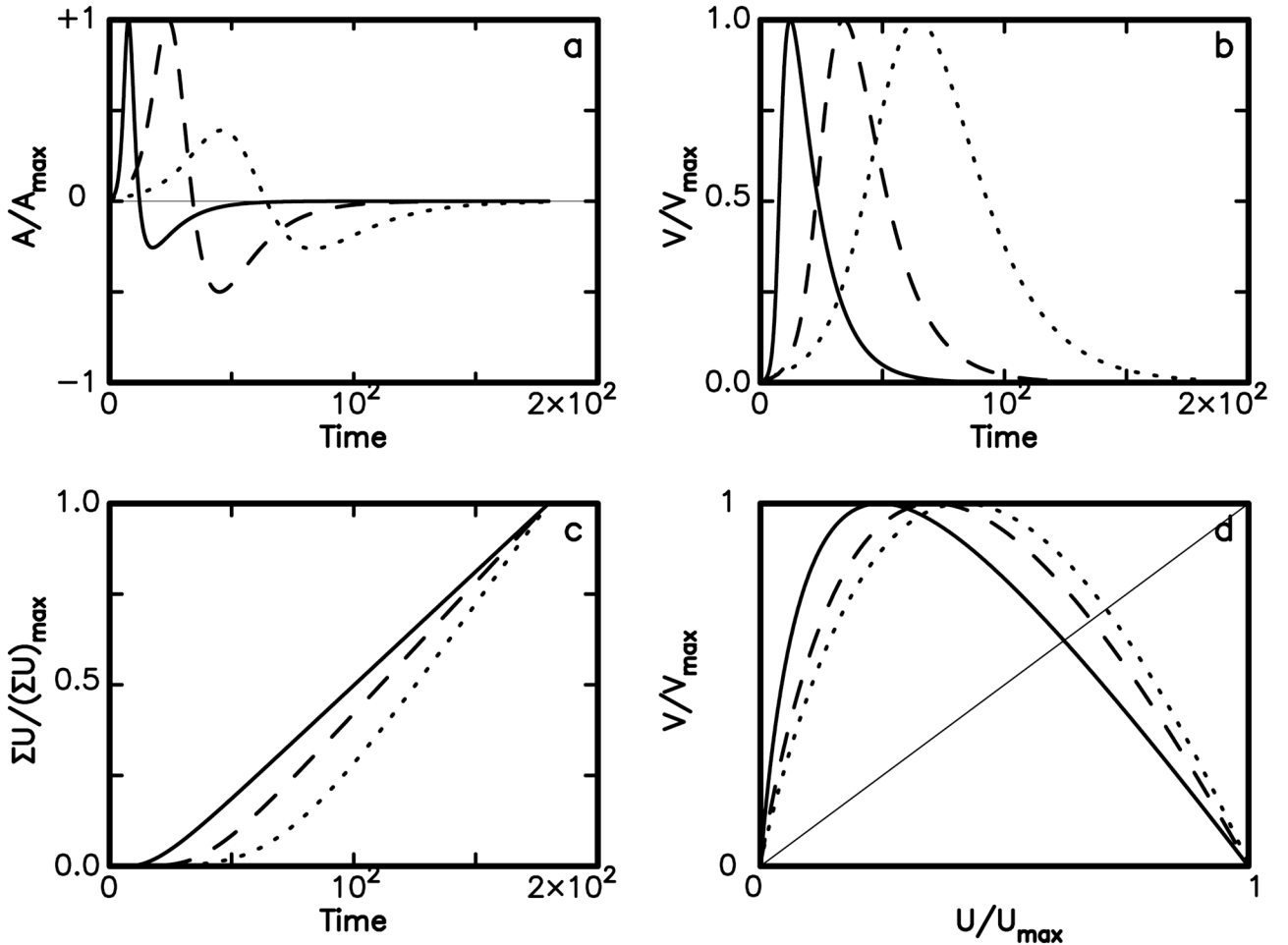
Figure 8. The time sequences of normalized acceleration (A/A_{max}), normalized velocity (V/V_{max}), and normalized cumulative displacement $\Sigma U/(\Sigma U)_{max}$ and the phase portrait of V/V_{max} versus U/U_{max} of the slider, acted by TP friction of $F(U) = \exp(-U/U_c)$, for $U_c = 0.1$ (solid line), 0.3 (dashed line), and 0.5 (dotted line) when $\eta = 10$.

line), 0.3 (dashed line), and 0.5 (dotted line) when $\eta = 10$. Figure 10 displays the time variations in A/A_{max}, V/V_{max}, and $\Sigma U/(\Sigma U)_{max}$ and the phase portrait of V/V_{max} versus U/U_{max} for the SH friction law with $U_c = 0.1$ (solid line), 0.3 (dashed line), and 0.5 (dotted line) when $\chi = 0.3$ and $\eta = 10$. Figures 8-10 exhibit the frictional effect.

5. Discussion

Analytic results at low velocities leads to Equation (9) which reveals the influences on slip of the slider by friction and viscosity. When $\gamma = 0$, Equation (9) demonstrates the slip of the slider specified by an exponentially damped sinusoidal function. Friction only lengthens the natural period of the system, T_n; while viscosity not only lengthens T_n but also makes the wave attenuated. When $\eta = 0$, Equation (9) expresses a purely sinusoidal wave.

Figure 5 shows that the time functions of displacements exhibit a sinusoidal function because of $\eta = 0$ and change with γ. Since the normalized displacement and $\eta = 0$ are considered, the peak amplitude does not change with γ. Actually, the displacement itself depends upon η and ω_n which are a function of γ, η, K, and m. The occurrence time of peak amplitude and the predominant period increase with γ. The initial changing rates of displacement with time are almost the same for the five values of γ. Results suggest that slip-weakening friction can influence slip of the slider.

Figure 6 exhibits that the time functions of displacements show a sinusoidal function (displayed by the upmost curve) when $\eta = 0$, and departs from a sinusoidal function when $\eta > 0$. The amplitude decreases with increasing η. Meanwhile, the peak amplitude appears earlier when η becomes larger. This might be due to a fact that attenuation of slip wave remarkably increases with η. Based on Equation (7), the predominant period should increase with η. This point cannot be clearly viewed from Figure 6 due to strong attenuation. Unlike Figure 5, the initial changing rate of displacement with time slightly decreases with increasing η. Results suggest that viscosity plays a significant role on slip of the slider. A comparison between Figure 5 and Figure 6 reveals that a change of η will result in a larger
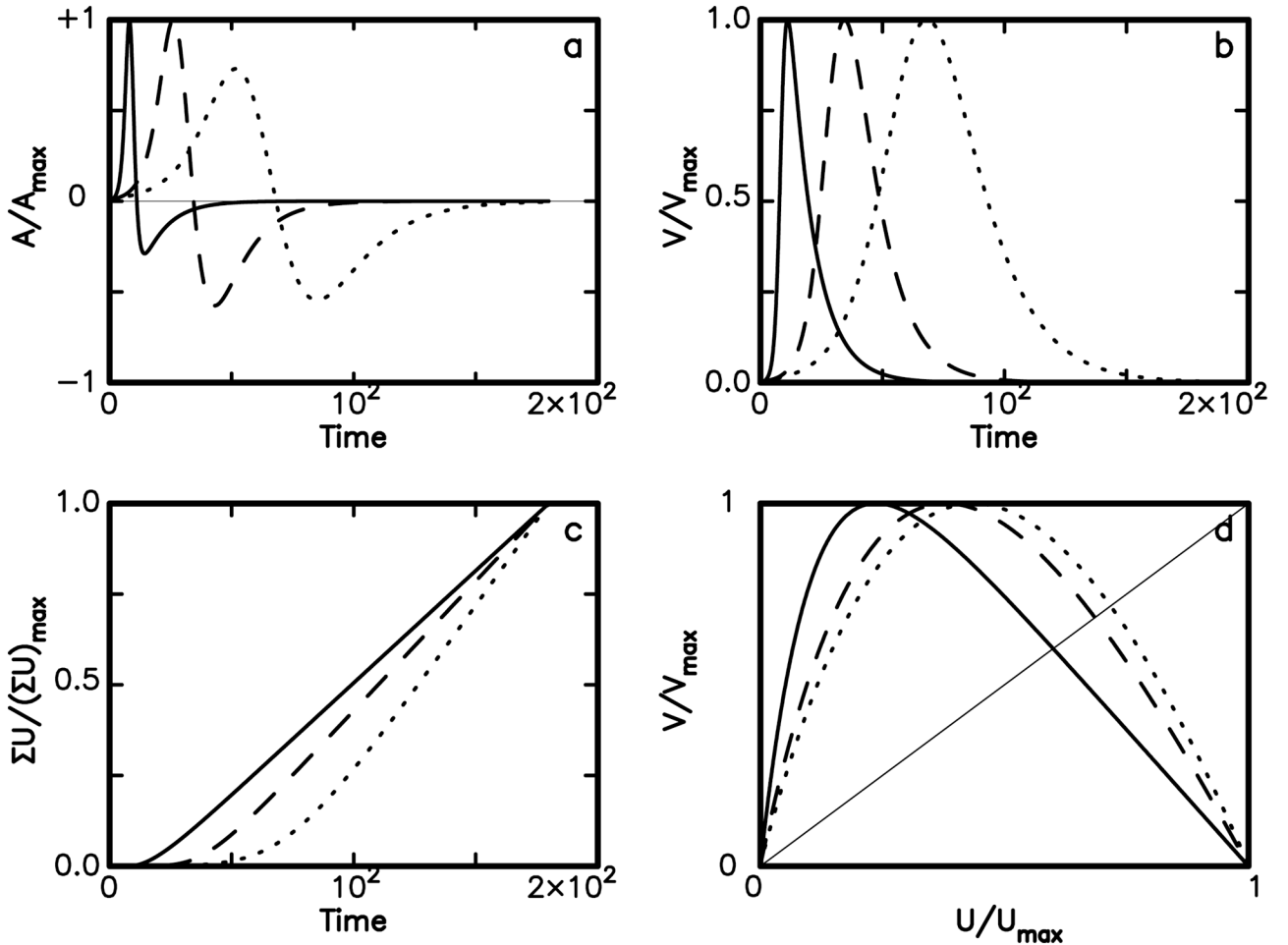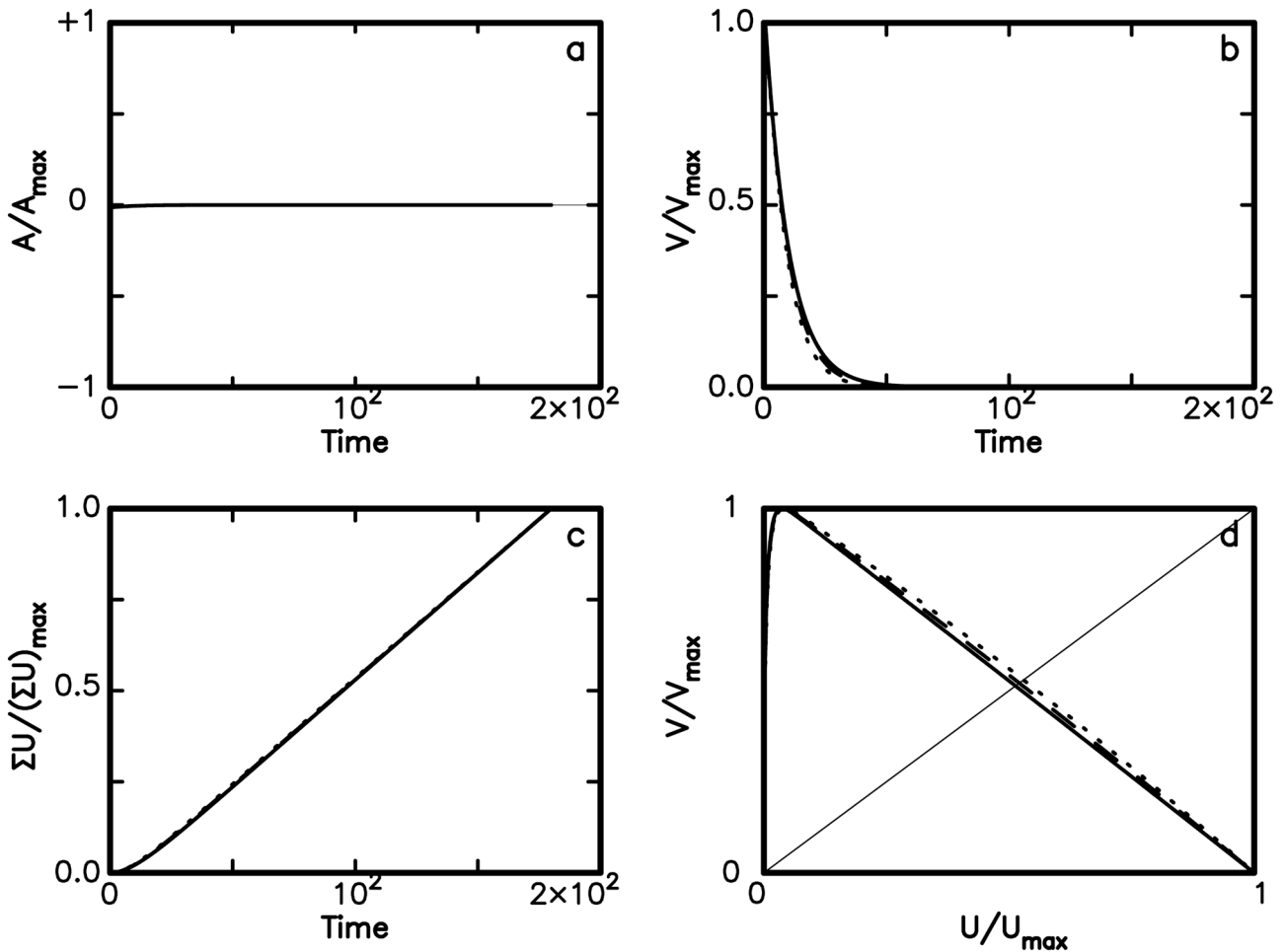

Figure 9. The time variations in normalized acceleration (A/A_{max}), normalized velocity (V/V_{max}), and normalized cummulative displacement $\Sigma U/(\Sigma U)_{max}$ and the phase portrait of V/V_{max} versus U/U_{max} of the slider, acted by SW friction of $F(U) = 1/(U+U_c)$, for $U_c = 0.1$ (solid line), 0.3 (dashed line), and 0.5 (dotted line) when $\eta = 10$.

effect on slip of the slider than a change of γ.

The viscous effect on slip of the slider in the presence of TW friction is displayed in Figure 7 which shows the time functions of A/A_{max}, V/V_{max}, and $\Sigma U/(\Sigma U)_{max}$ and the phase portrait of V/V_{max} versus U/U_{max} of the slider for $\eta =10$ (solid line), 20 (dashed line), and 30 (dotted line) when $U_c=0.1$. Figure 7a shows that the amplitude of A/A_{max} does not change with η, but the occurrence time of the amplitude increases with η. The predominant period of the time function of A/A_{max} increases with . Figure 7b shows that the amplitude of V/V_{max} does not change with η, but the occurrence times of the amplitude increase with η. The predominant period of the time function of V/V_{max} increases with U_c. Figure 7c shows that the value of $\Sigma U/(\Sigma U)_{max}$ decreases with increasing η. Figure 7d shows the phase portrait of V/V_{max} versus U/U_{max}. The three portraits are almost coincided. In the plot, the intersection points of the bisection line (denoted by a thin solid line) with the three curves are the fixed points. Although the slope is not calculated for each fixed point, the value can be estimated from

the plot. The absolute values of slope at the fixed points are almost the same and are likely all larger than 1, and thus the fixed points are not an attractor.

The frictional effects caused by three different slip-weakening friction laws in consideration are displayed in Figures 8-10. Figure 8 shows the time functions in A/A_{max}, V/V_{max}, and $\Sigma U/(\Sigma U)_{max}$ and the phase portrait of V/V_{max} versus U/U_{max} of the slider, acted by TW friction, for $U_c=0.1$ (solid line), 0.3 (dashed line), and 0.5 (dotted line) when $\eta =10$. Figure 8a shows that the amplitude of A/A_{max} obviously change with U_c, and the occurrence time of the amplitude increases with U_c. The predominant period of the time function of A/A_{max} increases with U_c. Figure 8b shows that the amplitude of V/V_{max} does not change with U_c, but the occurrence time of the amplitude increases with U_c. The predominant period of the time function of V/V_{max} increases with U_c. Figure 8c shows that the value of $\Sigma U/(\Sigma U)_{max}$ decreases with increasing U_c. Figure 8d shows the phase portrait of V/V_{max} versus U/U_{max}. In the plot, the intersection point of the bisection line (denoted by a thin solid line) with each of the three curves

Figure 10. The time variations in normalized acceleration (A/A_{max}), normalized velocity (V/V_{max}), and normalized cumulative displacement $\Sigma U/(\Sigma U)_{max}$ and the phase portrait of V/V_{max} versus U/U_{max} of the slider, acted by SW friction of $F(U) = \exp[-(U^2-U_c^2)/\chi^2]$, for $U_c=$ 0.1 (solid line), 0.3 (dashed line), and 0.5 (dotted line) when $\chi = 0.3$ and $\eta = 10$.

is the fixed point. Although the slope is not calculated for each fixed point, the value can be estimated from the plot. The absolute values of slope at the fixed points increases with U_c and are all larger than 1. Hence, the fixed points are not an attractor.

Figure 9 shows the time functions in A/A_{max}, V/V_{max}, and $\Sigma U/(\Sigma U)_{max}$ and the phase portrait of V/V_{max} versus U/U_{max} of the slider, acted by SW friction, for $U_c = 0.1$ (solid line), 0.3 (dashed line), and 0.5 (dotted line) when $\eta = 10$. Figure 9a shows that the amplitude of A/A_{max} changes with U_c, and the occurrence time of the amplitude increases with U_c. The predominant period of the time function of A/A_{max} increases with U_c. Figure 9b shows that the amplitude of V/V_{max} does not change with U_c, and the occurrence time of the amplitude increases with U_c. The predominant period of the time function of V/V_{max} increases with U_c. Figure 9c shows that the value of $\Sigma U/(\Sigma U)_{max}$ decreases with increasing U_c. Figure 9d shows the phase portrait of V/V_{max} versus U/U_{max}. In the plot, the intersection point of the bisection line (denoted by a thin solid line) with each of the three curves is the fixed point. Although the slope is not calculated for each fixed point, the value can be estimated from the plot. The absolute values of slope at the fixed points increases with U_c and are all larger than 1. Hence, the fixed points are not an attractor. A comparison between Figure 8 and Figure 9 suggests that the TP and SW friction laws likely make similar effects on earthquake ruptures. This might be due to similar variations in friction force with slip for the two friction laws as displayed in Figure 3.

Figure 10 shows the time functions in A/A_{max}, V/V_{max}, and $\Sigma U/(\Sigma U)_{max}$ and the phase portrait of V/V_{max} versus U/U_{max} of the slider, acted by SW friction, for $U_c = 0.1$ (solid line), 0.3 (dashed line), and 0.5 (dotted line) when $\eta = 10$. Unlike Figures 7-9, Figure 10a shows that A/A_{max} drops suddenly from an initial value to zero and almost does not change with U_c. Figure 10b shows that the time functions of V/V_{max} and the occurrence times of the peak value of V/V_{max} do not change with U_c. Figure 10c shows that the time functions of $\Sigma U/(\Sigma U)_{max}$ only slightly increases with U_c. Figure 10d shows that the phase portraits of V/V_{max} versus U/U_{max} for the three values of U_c are almost the same and form a line intersecting the bisection line. at the respective fixed points. The three fixed points are almost the same. Although the slope is not calculated for each fixed point, the value can be estimated from the plot. The absolute values of slope at the fixed points are likely all slightly larger than 1, and thus the fixed points are not an attractor. In addition, the plots in Figure 10 are quite different from those in Figures 8-9. This might be due to a fact that the SW

friction law is quite different from the other two as displayed in Figure 3.

6. Conclusions

In order to study the effects on earthquake ruptures caused by slip-weakening friction and viscosity, the slip of a one-body dynamical slider-slider model is theoretically analyzed and numerically simulated when the two factors are present. Analytic results with numerical computations show that the displacement of the slider is controlled by the decreasing rate, γ, of friction force with slip and viscosity, η, of fault-zone material. The natural period of the system with slip-weakening friction and viscosity is longer than that of the system without the two factors. There is a solution regime controlled by the parabolic equation of $\eta^2 + 4m\gamma = 4mK$ to result in stable slippage of the slider. Meanwhile, a change of η will result in a larger effect on slip of the slider than a change of γ.

Numerical simulations lead to the time functions in A/A_{max}, V/V_{max}, and $\Sigma U/(\Sigma U)_{max}$ and the phase portrait of V/V_{max} versus U/U_{max} of the slider in the presence of three slip-weakening friction laws, i.e., the thermal-pressurization (TP) friction law, the softening-hardening (SH) friction law, and a simple slip-weakening (SW) friction law, and viscosity. Results show that slip-weakening friction and viscosity remarkably affect the three time functions and phase portrait. The TP and SW friction laws cause very similar results. The results caused by the SH friction laws are quite different from those by the other two. For all cases in study, the fixed points are not an attractor.

References

Ampuero, J.P., and A.M. Rubin (2008). Earthquake nucleation on rate and state faults - Aging and slip laws, J. Geophys. Res., 113, B01302; doi:10.1029/2007JB005082.

Anderson, O.L., and P.C. Grew (1977). Stress corrosion theory of crack propagation with applications to geophysics, Rev. Geophys. Space Phys., 15, 7-104.

Atkinson, B.K. (1984). Subcritical crack growth in geological materials, J. Geophys. Res., 89, 4077-4114.

Beeler, N.M., T.E. Tullis and D.L. Goldsby (2008). Constitutive relationships and physical basis of fault strength due to flash heating, J. Geophys. Res., 113,

B01401; doi:10.1029/2007JB004988.

Bhattacharya, A. and A.M. Rubin (2014). Frictional response to velocity steps and 1-D fault nucleation under a state evolution law with stressing-rate dependence, J. Geophys. Res. Solid Earth, 119, 2272-2304; doi:10.1002/2013JB010671.

Bizzarri, A., and M. Cocco (2006a). A thermal pressurization model for the spontaneous dynamic rupture propagation on a three-dimensional fault: 1. Methodological approach, J. Geophys. Res., 111, B05303; doi:10.1029/2005JB003862.

Bizzarri, A., and M. Cocco (2006b). A thermal pressurization model for the spontaneous dynamic rupture propagation on a three-dimensional fault: 2. Traction evolution and dynamic parameters, J. Geophys. Res., 111, B05304; doi:10.1029/2005JB003864.

Bizzarri, A., and M. Cocco (2006c). A thermal pressurization model for the spontaneous dynamic rupture propagation on a three-dimensional fault: 2. Traction evolution and dynamic parameters, J. Geophys. Res., 111, B05304; doi:10.1029/2005JB003864.

Bizzarri, A. (2009). Can flash heating of asperity contacts prevent melting?, Geophys. Res. Lett., 36, L11304; doi:10.1029/2009GL037335.

Bizzarri, A. (2010). An efficient mechanism to avert frictional melts during seismic ruptures, Earth Planet. Sci. Lett., 296, 144-152; doi:10.1016/j.epsl.2010.05.012.

Bizzarri, A. (2011a). Dynamic seismic ruptures on melting fault zones, J. Geophys. Res., 116, B02310; doi: 10.1029/2010JB007724.

Bizzarri, A. (2011b). Temperature variations of constitutive parameters can significantly affect the fault dynamics, Earth Planet. Sci. Lett., 306, 72-278; doi: 10.1016/j.epsl.2011.04.009.

Bizzarri, A. (2011c). On the deterministic description of earthquakes, Rev. Geophys., 49, RG3002; doi:10.1029/2011RG000356.

Bizzarri, A., and P. Crupi (2013). Is the initial thermal state of a fault relevant to its dynamic behavior?, B. Seismol. Soc. Am., 103 (3), 2062-2069; doi:10.1785/0120120279.

Brantut, N., J. Sulem and A. Schubnel (2011). Effect of dehydration reactions on earthquake nucleation: Stable sliding, slow transients, and unstable slip, J. Geophys. Res., 116, B05304.

Brodsky, E.E., and H. Kanamori (2001). Elastohydrodynamic lubrication of faults, J. Geophys. Res., 106, 16357-16374.

Brune, J. (1979). Implications of earthquake triggering and rupture propagation for earthquake prediction based on premonitory phenomena, J. Geophys. Res., 84, 2195-2198.

Burridge, R., and L. Knopoff (1967). Model and theoretical seismicity, B. Seismol. Soc. Am., 57, 341-371.

Byerlee, J.D. (1968). Brittle-ductile transition in rocks, J. Geophys. Res., 73, 4711-4750.

Byerlee, J. (1978). Friction of rocks, Pure. Appl. Geophys., 116, 615-626.

Cao, T., and K. Aki (1984/85). Seismicity simulation with a mass-spring model and a displacement hardening-softening friction law, Pure. Appl. Geophys., 122, 10-24.

Cao, T., and K. Aki (1986). Seismicity simulation with a rate- and state-dependent friction law, Pure Appl. Geophys., 124, 487-513.

Carlson, J.M., and J.S. Langer (1989). Mechanical model of an earthquake fault, Phys. Rev. A, 40, 6470-6484.

Carlson, J.M. (1991). Time intervals between characteristic earthquakes and correlation with smaller events: An analysis based on a mechanical model of a fault, J. Geophys. Res., 96, 4255-4267.

Carlson, J.M., J.S. Langer, B.E. Shaw and C. Tang (1991). Intrinsic properties of a Burridge-Knopoff model of an earthquake fault, Phys. Rev. A, 44, 884-897.

Chester, F.M., and H.G. Higgs (1992). Multimechanism friction constitutive model for ultrafine quartz gouge at hypocentral conditions, J. Geophys. Res., 97, B2, 1859-1870.

Cochard, A., and R. Madariaga (1994). Dynamic faulting under rate-dependent friction, Pure Appl. Geophys., 142, 419-445; doi:10.1007/BF00876049.

Cohen, S. (1979). Numerical and laboratory simulation of fault motion and earthquake occurrence, Rev. Geophys. Space Phys., 17 (1), 61-72

Dieterich, J.H. (1972). Time-dependent friction in rocks, J. Geophys. Res., 77 (20), 3690-3697.

Dieterich, J.H. (1979). Modeling of rock friction 1. Experimental results and constitutive equations, J. Geophys. Res., 84, 2161-2168.

Dragoni, M., and S. Santini (2015). A two-asperity fault model with wave radiation, Phys. Earth Planet. Int., 248, 83-93.

Fang, Z., J.H. Dieterich, K.B. Richards-Dinger and G. Xu (2011). Earthquake nucleation on faults with nonconstant normal stress, J. Geophys. Res., 116, B09307; doi:10.1029/2011JB008196.

Fialko, Y.A. (2004). Temperature fields generated by the elastodynamic propagation of shear cracks in the Earth, J. Geophys. Res., 109, B01303; doi:10.1029/2003JB002496.

Garagash, D.I., and L.N. Germanovich (2012). Nucleation and arrest of dynamic slip on a pressurized fault, J. Geophys. Res., 117, B10310; doi:10.1029/2012JB009209.

Hudson, J.A. (1980). The excitation and propagation of elastic waves, Cambridge Monographs on Mechan-

ics and Applied Mathematics, Cambridge Univ. Press, 224 p.

Jeffreys, H. (1942). On the mechanics of faulting, Geol. Mag., 79, 291.

Kano, Y., J. Mori, R. Fujio, H. Ito, T. Yanagidani, S. Nakao and K.F. Ma (2006). Heat signature on the Chelungpu fault associated with the 1999 Chi-Chi, Taiwan, earthquake, Geophys. Res. Lett., 33, L14306; doi:10.1029/2006GL026733.

Kittel, C., W.D. Knight and M.A. Ruderman (1968). Mechanics, Berkeley Physics Course Volume 1, Mc-Graw-Hill Book Co., New York, N.Y., 480 p.

Knopoff, L., J.Q. Mouton and R. Burridge (1973). The dynamics of a one-dimensional fault in the presence of friction, Geophys. J. R. astro. Soc., 35, 169-184.

Knopoff, L., J.A. Landoni and M.S. Abinante (1992). Dynamical model of an earthquake fault with localization, Phys. Rev. A, 46, 7445-7449.

Knopoff, L., and X.X. Ni (2001). Numerical instability at the edge of a dynamic fracture, Geophys. J. Int., 147, F1-F6.

Lachenbruch, A.H. (1980). Frictional heating, fluid pressure, and the resistance to fault motion, J. Geophys. Res., 85, 6097-6122.

Madariaga, R., and A. Cochard (1994). Seismic source dynamics, heterogeneity and friction, Annali di Geofisica, 37 (6), 1349-1375.

Marone, C. (1998). Laboratory-derived friction laws and their application to seismic faulting, Ann. Rev. Earth Planet. Sci., 26, 643-669.

Nur, A. (1978). Nonuniform friction as a physical basis for earthquake mechanics, Pure Appl. Geophys., 116, 964-989.

Ohnaka, M. (2003). A constitutive scaling law and a unified comprehension for frictional slip failure, shear fracture of intact rocks, and earthquake rupture, J. Geophys. Res., 108 (B2), 2080; doi:10.1029/2000JB000123.

Press, W.H., B.P. Flannery, S.A. Teukolsky and W.T. Vetterling (1986). Numerical Recipes, Cambridge Univ. Press, Cambridge, 818 p.

Rice, J.R. (1993). Spatio-temporal complexity of slip on a fault, J. Geophys. Res., 98 (B6), 9885-9907.

Rice, J.R., N. Lapusta and K. Ranjith (2001). Rate and state dependent friction and the stability of sliding between elastically deformable solids, J. Mech. Phys. Solids, 49, 1865-1898.

Rice, J.R. (2006). Heating and weakening of faults during earthquake slip, J. Geophys. Res., 111, B05311; doi:10.1029/2005JB004006.

Rubin, A.M., and J.P. Ampuero (2005). Earthquake nucleation on (aging) rate and state faults, J. Geophys. Res., 110, B11312; doi:10.1029/2005JB003686.

Ruina, A.L. (1983). Slip instability and state variable friction laws, J. Geophys. Res., 88, 10,359-10,370.

Scholz, C.H. (1990). The Mechanics of Earthquakes and Faulting, Cambridge Univ. Press, Cambridge, 439 p.

Shimamoto, T. (1986). Strengthening of phyllosilicate and gypsum gouges with increasing temperature: effect of temperature or moisture elimination?, Int. J. Rock Mech. Min. Sci. & Geomech. Abstr., 123, 439-443.

Sibson, R.H. (1973). Interaction between temperature and pore-fluid pressure during earthquake faulting and a mechanism for partial or total stress relief, Natural Phys. Sci., 243, 66-68.

Sibson, R.H. (1975). Generation of pseudotachylite by ancient seismic faulting, Geophys. J. Roy. Astr. Soc., 43, 775-794.

Sibson, R.H. (2003). Thickness of the seismic slip zone, B. Seismol. Soc. Am., 93, 1169-1178.

Sone, H., and T. Shimamoto (2009). Frictional resistance of faults during accelerating and decelerating earthquake slip, Nat. Geosci., 2, 705-708; doi:10.1038/ngeo637.

Spray, J.G. (1993). Viscosity determinations of some frictionally generated silicate melts: Implications for fault zone rheology at high strain rates, J. Geophys. Res., 98 (B5), 8053-8068.

Spray, J.G. (1995). Pseudotachylyte controversy: Fact or friction?, Geology, 23 (12), 1119-1122.

Spray, J.G. (2005). Evidence for melt lubrication during large earthquakes, Geophys. Res. Lett., 32, L07301; doi:10.1029/2004GL022293.

Thompson, J.M.T., and H.B. Stewart (1986). Nonlinear Dynamics and Chaos, John Wiley and Sons, New York, 376 p.

Turcotte, D.L., and G. Schubert (1982). GEODYNAMICS - Applications of Continuum Physics to Geological Problems, Wiley, 450 p.

Wang, J.H. (1995). Effect of seismic coupling on the scaling of seismicity, Geophys. J. Int., 121, 475-488.

Wang, J.H. (1996). Velocity-weakening friction law as a factor in controlling the frequency-magnitude relation of earthquakes, B. Seismol. Soc. Am., 86, 701-713.

Wang, J.H. (1997). Effect of frictional healing on the scaling of seismicity, Geophys. Res. Lett., 24, 2527-2530.

Wang, J.H., and R.D. Hwang (2001). One-dimensional dynamical simulations of slip complexity of earthquake faults, Earth Planets Space, 53, 91-100.

Wang, J.H. (2002). A dynamical study of comparing two one-variable, rate- dependent and state-dependent friction laws, B. Seismol. Soc. Am., 92, 687-694.

Wang, J.H. (2006). Energy release and heat generation during the 1999 Chi-Chi, Taiwan, earthquake, J. Geophys. Res., 111, B11312; doi:10.1029/2005JB004018.

Wang, J.H. (2007). A dynamic study of the frictional and

viscous effects on earthquake rupture: a case study of the 1999 Chi-Chi earthquake, Taiwan, B. Seismol. Soc. Am., 97 (4), 1233-1244.

Wang, J.H. (2008). One-dimensional dynamical modeling of earthquakes: A review, Terr. Atmos. Ocean. Sci., 19, 183-203.

Wang, J.H. (2009). Effect of thermal pressurization on the radiation efficiency, B. Seismol. Soc. Am., 99 (4), 2293-2304.

Wang, J.H. (2011). Thermal and pore fluid pressure history on the Chelungpu fault at a depth of 1111 meters during the 1999 Chi-Chi, Taiwan, earthquake, J. Geophys. Res., 116, B03302; doi:10.1029/2010JB007765.

Wang, J.H. (2012). Some intrinsic properties of the two-dimensional dynamical spring-slider model of earthquake faults, B. Seismol. Soc. Am., 102 (2), 822-835.

Wang, J.H. (2013). Stability analysis of slip of a one-body spring-slider model in the presence of thermal pressurization, Annals of Geophysics, 56 (3), R03332; doi:10.4401/ag-5548.

Wang, J.H. (2016). A dynamical study of frictional effect on scaling of earthquake source displacement spectra, Annals of Geophysics, 59 (2), S0210, 1-14; doi: 10.4401/ag-6974.

Xu, H.J., and L. Knopoff (1994). Periodicity and chaos in a one-dimensional dynamical model of earthquakes, Phys. Rev. E, 50 (5), 3577-3581.

Corresponding author: Jeen-Hwa Wang,
Institute of Earth Sciences, Academia Sinica, Taipei, Taiwan;
email: jhwang@earth.sinica.edu.tw.